Water Research 170 (2020) 115384

Contents lists available at ScienceDirect

Water Research

journal homepage: www.elsevier.com/locate/watres

Modeling cell aggregate morphology during aerobic granulation in activated sludge processes reveals the combined effect of substrate and shear

Jun Wu [a, *], Francis L. de los Reyes III [b], Joel J. Ducoste [b]

[a] School of Environmental Engineering and Science, Yangzhou University, 196 West Huayang Road, Yangzhou, Jiangsu, 225127, China
[b] Department of Civil, Construction, and Environmental Engineering, North Carolina State University, Campus Box 7908, Raleigh, NC, 27695-7908, United States

ARTICLE INFO

Article history:
Received 31 July 2019
Received in revised form
5 November 2019
Accepted 8 December 2019
Available online 9 December 2019

Keywords:
Aerobic granular sludge
Computational fluid dynamics
Substrate transport
Activated sludge
Biofilm modelling

ABSTRACT

Past research on AGS (aerobic granular sludge technology) has mainly focused on macro-environment factors, such as settling time, feeding pattern, OLR (organic loading rate), SRT (sludge retention time), among others, and their effects on the granulation process. The biomass granulation process, however, is significantly affected by the micro-environment surrounding these biomass aggregates. In this research, an *in silico* computational approach was adopted to study the impact of the micro-environment on the biomass granulation process. A 2-D biofilm model based on the cellular automata algorithm and computational fluid dynamics was used to simulate the development of an individual biomass aggregate under specific hydrodynamic and substrate availability conditions. The simulation results indicated that shear and bulk substrate concentration combined to create the optimal conditions for aerobic granule formation. This process can be characterized by the RT (reversed Thiele) modulus value, which is the ratio of the maximum substrate transport over the maximum substrate reaction rate and an indicator of substrate availability. For AGS formation, the RT value should be greater than 0.1. Many common strategies, such as the application of batch reactors, selection for slow-growing microorganism, F/M (food/mass) ratio adjustment, feast and famine condition, and short settling time, for biomass granulation production can be explained by the RT value. The results suggest that rethinking unit process configurations in wastewater treatment facilities will be required to achieve reliable AGS formation.

1. Introduction

Because of its many advantages, AGS (aerobic granular sludge) technology for wastewater treatment has been the subject of increasing research focus in the past two decades (Beun et al., 1999; Franca et al., 2018). In AGS systems, the biomass aggregate into self-immobilized large dense granules with sizes between 200 and 2000 μm (Beun et al., 2002), while in CAS (conventional activated sludge), the biomass forms smaller flocs. Aerobic granules settle faster than CAS flocs, allowing for more efficient settling, higher treatment efficiency, and compact plant design. Moreover, the stratified layers of aerobic, anoxic, and anaerobic conditions in the radial direction of the granules allow for potential simultaneous removal of organic material, nitrogen, and phosphorous (de Kreuk et al., 2005).

While past research has revealed operational conditions associated with granular sludge formation, the mechanisms involved in their formation and disintegration are still not fully understood (Nancharaiah and Reddy, 2018). Among many factors, the selective pressure from the short settling time in SBRs (sequencing batch reactors), hydrodynamic shear force, feeding pattern (i.e., feast-famine cycle, anaerobic feeding), F/M (food to mass) ratio, substrate type and concentration, OLR (organic loading rate), SRT (sludge retention time), and DO (dissolved oxygen) concentration have been considered the primary factors for granule formation and disintegration (Nancharaiah and Reddy, 2018). In addition, concerns with the long startup period for full-scale treatment (Pronk et al., 2015) and long term granule stability still hinder the wide application of AGS technology (Franca et al., 2018). Finally, the formation of AGS primarily in SBRs has also prevented the

* Corresponding author.
E-mail address: j.wu@yzu.edu.cn (J. Wu).

https://doi.org/10.1016/j.watres.2019.115384
0043-1354/

incorporation of AGS technology in wastewater treatment as these systems are not easily applied in continuous flow wastewater treatment facilities (Kent et al., 2018).

Many of these factors influencing biomass granulation deal with the macro-environment at the reactor-scale. Yet, it is the micro-environment surrounding the single biomass aggregates that determines the biomass granulation process, and many mechanistic models for biomass granulation, i.e., inert nuclei model, selection pressure model, multi-valence positive ion-bonding model, etc., were developed on the micro-scale (Liu et al., 2003). While the macro-environment affects the micro-environment for the biomass aggregates, the degree to which the macro-environment affects this micro-environment varies. For example, the hydrodynamic shear force imposed by the same aeration rate could cause entirely different micro-environments for different reactor configurations. The OLR, F/M ratio, and DO could have different effects on the substrate concentrations at the micro-scale for biomass aggregates of different sizes, density, viable biomass content, and growth rate.

Examining the individual micro-environment for single biomass aggregates is very difficult to perform through laboratory experiments. *Particle image velocimetry has been attempted to measure the flow velocity field in a fixed biofilm system* (Stoodley et al., 1994). *However, there are no experimental methods to characterize the flow condition around suspended growth granules. Some specific substrate concentrations (i.e., DO, nitrite, and nitrate) within granules were measured using microelectrodes that are mounted on precisely controlled devices* (Li and Bishop, 2004). *Unfortunately, the obtrusive nature of using microelectrodes may affect the actual micro-environment that influence substrate transport and the local cultivation of these biomass aggregates*. Many of the factors involved in biomass granulation are indeed interrelated. For example, both the hydrodynamic shear force and substrate loading rate impact the substrate transport around the surface of the biomass aggregates (Liu and Tay, 2002). The two factors were not easily separable.

In this research, an *in silico* computational approach was adopted to study the impact of the micro-environment on the biomass granulation process. A 2-D biofilm model based on the cellular automata algorithm and computational fluid dynamics was used to simulate the development of the individual biomass aggregate under specific substrate availability and hydrodynamic conditions. The substrate availability was included as it directly affects the biomass growth rate. The hydrodynamic condition could affect the transport of substrate to biomass along with the aggregate solids detachment process.

The simulation tools developed in this study are expected to assist experimental investigations and provide insight into the biomass aggregation process at the micro-scale level. In particular, this paper aims to answer the following research questions:

(1) What favorable micro-environments lead to the formation of granules, i.e., how do the substrate concentration and hydrodynamic shear surrounding the biomass aggregates affect the granulation process?
(2) Is there a unique combination of substrate concentration and hydrodynamic shear that determines the biomass granulation process?
(3) Can these simulations explain the main experimental results, i.e., why biomass granulation is more prevalent in SBRs than in continuous flow reactors?
(4) What are the possible operational strategies at the reactor macro level to achieve a favorable micro-environment for the formation of AGS?

2. Model description

2.1. Model geometry and setup

A two-dimensional FEM (finite element model) that includes biomass aggregate formation (growth), liquid flow, soluble substrate transport (both convective and diffusive), biodegradation, and detachment was developed. A singular biomass aggregate was tracked in a rectangular flow field with a width and height of 20 mm and 15 mm, respectively (Fig. 1). The left and right edges of this flow field were defined as the inlet and outlet as shown in Fig. 1. The inlet liquid velocities were varied to study the effect of shear on biomass aggregation. Shear forces produced from varying the inlet liquid velocities ranged between 0 and 250 s^{-1}. The top and bottom edges of the flow domain were defined as symmetrical boundaries to minimize the impact of rectangle height on the simulation results. The simulated biomass aggregate was composed of multiple $10 \times 10\ \mu m$ computational cells. A sensitivity analysis of the computational cell size was performed to confirm that the computational cell size has no significant impact on the simulation results in terms of the granule and floc morphology, i.e., circularity (results shown in the Supplementary Information (SI), Figs. S1 and S2). The size and shape of the biomass aggregate were developed from the total number and the position of these cells, which were determined through the cellular automata algorithms for biomass development described in Section 2.4. The biomass aggregate was allowed to rotate in the flow field at 15°increments in each simulation interval to imitate the potential movement of biomass aggregates in the flow field.

The biomass aggregate was surrounded by a CBL (concentration boundary layer) and a HBL (hydraulic boundary layer) as suggested by Bishop et al. (1997). A schematic representation of the CBL and HBL is shown in Fig. S3. The CBL is a region above the biomass aggregate where the flow is assumed stagnant. The HBL is a region in which the flow velocity reduces from the free-stream velocity to zero at the top of CBL. The border of the CBL was defined by a circle located at the centroid of the biomass aggregate. The radius of the CBL circle is the sum of the radius of the minimum bounding circle for the biomass aggregate and the CBL thickness. The HBL circle was the concentric circle of the CBL and had a radius that is the sum of CBL radius and HBL thickness. According to experimental results from Bishop et al. (1997), the thickness of the CBL (in μm) depends on the flow velocity (m/s) (Eq. (1)) while the thickness of the HBL equals 4.8 mm, which was not affected by the biofilm roughness and only slightly influenced at different flow velocities (Bishop et al., 1997).

$$L_C = 200 + 800e^{-200V} \quad (1)$$

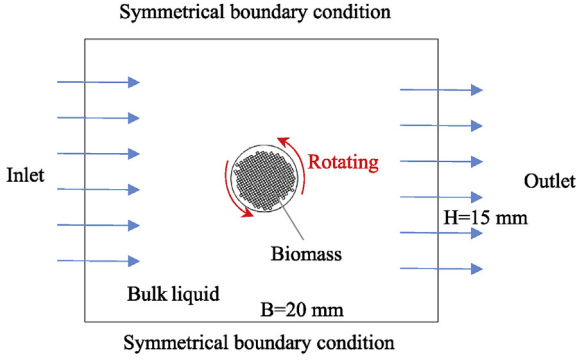

Fig. 1. Model setup for simulation of biomass floc/granule formation under different shear and substrate conditions.

Four distinct regions: bulk liquid, HBL, CBL and biomass aggregates, were modeled with different governing equations described in Section 2.3. The bulk liquid was the area outside the HBL. The mass transfer in the HBL was simulated by including advection and diffusion. Since the flow in the CBL is stagnant, the mass transfer in the CBL was simulated by diffusion alone. The substrate concentration inside the biomass aggregates was simulated by diffusion and reaction (i.e., convective transport was not included (Wanner and Morgenroth, 2004)).

2.2. Hydraulic modeling

The water flow in the bulk liquid and HBL was simulated using the Navier–Stokes equations assuming laminar flow. The maximum inlet velocity was set to 0.05 m/s. The maximum Re (Reynolds number) was 500 (assuming a water density = 1000 kg/m^3, dynamic viscosity = 0.001 Pa-S and water flow height = 10 mm). The inlet velocity varied between 0 and 0.05 m/s, which produced an average shear rate in the vicinity of a 0.5 mm diameter granule between 0 and 250 s^{-1}. Fig. S4(a) in the SI displays the distribution of shear rate around the 0.5 mm granule with an inlet velocity of 0.05 m/s. Fig. S4(b) shows the correlation between the inlet velocity and the average shear rate. A no-slip boundary condition was defined for the biomass aggregate surface and a zero pressure condition was adopted for the outlet of the hydraulic simulation domain. The shear stress calculated from the hydraulic model was used to control the detachment of granules. Biomass detachment was initiated when the shear stress was higher than 0.5 Pa (Stoodley et al., 1999). The flow velocity was used to calculate the convective transport of the substrate within the HBL.

2.3. Soluble substrate mass balance

The soluble substrate transport in the HBL was simulated using the convective and diffusive transport equation:

$$\frac{\partial S}{\partial t} = D_l \nabla^2 S - u \nabla S \tag{2}$$

where, D_l is the diffusion coefficient in the liquid, u is the flow velocity calculated from the hydraulic modeling, and S is the soluble substrate concentration. The bulk liquid was assumed to be completely mixed. The constant substrate concentration boundary condition was applied at the interface between the HBL and bulk liquid.

The soluble substrate mass balance in the biomass aggregates was simulated using the diffusion-reaction equation:

$$\frac{\partial S}{\partial t} = D_b \nabla^2 S + r_s \tag{3}$$

where, D_b is the diffusional coefficient in the biomass aggregates and r_s is the bioreaction rate, which can be expressed with eq. 4

$$r_s = \mu_{max,H} \frac{S}{S + K_S} X \tag{4}$$

where, $\mu_{max,H}$ is the maximum specific biomass growth rate (d^{-1}), X is the biomass concentration (mg/L) and K_S is the substrate half-saturation constant (mg/L). In the ASM (activated sludge models), several substrate limitation conditions were used. For simplicity, only one limiting substrate (organic matter) was used in this study. The values of the model parameters used in eqs. (2)–(4) were obtained from the literature (Table S1 in the SI).

2.4. Development of the biomass aggregate

A cellular automata algorithm was used for simulating the development of the biomass aggregate. The increase in the biomass concentration (ΔX) was calculated incrementally at a simulation duration of 6 h (ΔT) using the following equation:

$$\Delta X = Y_H \int_{T}^{T+\Delta T} r_s \tag{5}$$

where, Y_H was the yield coefficient of biomass due to substrate consumption. For simplicity, biomass decay was ignored.

Biomass was designed to spread from its starting location when the 10 × 10 μm cells split according to the CA (cellular automata) algorithm (Picioreanu et al., 1998). An 8-neighbor cell filling rule was used in the CA algorithm. The CA procedure consists of the following:

(a) If the biomass density in a cell reaches the critical density, X_C (Table S1), the biomass in the cell split into two equal parts. One part stayed in the original cell. The other half was placed randomly in one of the empty neighboring cells. The biomass density in the two split cells was adjusted to half of the original cell.
(b) If none of the 8 neighboring cells was empty, one of the 8 occupied cells was randomly chosen and the biomass inside the occupied cell was randomly displaced to one of its empty neighboring cells.
(c) If there were no empty neighboring cells from step (b), then step (b) was repeated until an empty cell was identified.
(d) The steps from (a) to (c) were executed repeatedly until the biomass density in all the cells was less than the critical density, X_C.

To examine the effect of simulation interval on the simulation results, a sensitivity analysis was performed using the simulation interval of 1, 2, 4, 6, and 12 h. Fig. S5 in the SI displays the derived granule images and circularities produced from simulations with different time intervals. The results in Fig. S5 show that the simulation interval had no significant effect on the biomass aggregate morphology and circularity. The detachment of biomass from the biomass aggregates was controlled by the shear stress calculated from the hydraulic model. Biomass detachment occurred when the surrounding shear stress exceeded 0.5 Pa, a value selected based on the measured biomass strength from (Stoodley et al., 1999).

2.5. Model implementation

The model was implemented in the MATLAB® 8.4 and COMSOL Multiphysics®5.2 environment. The main script was written in MATLAB to (1) define the model parameters, (2) call for the COMSOL solver, (3) define the model geometry, (4) solve the CA algorithm and (5) perform the biomass aggregates image analysis. The COMSOL software was used to solve the hydraulic and substrate mass balance partial differential equation (PDEs). The MATLAB and COMSOL software were integrated using the LiveLink™ feature of COMSOL for MATLAB. To reduce the impact of selected kinetic parameters on the simulation result, the bulk COD concentration was normalized to a minimum unit substrate, S_{min}, defined by the following equation:

$$S_{min} = \frac{K_S}{\mu_{max,H}} \tag{6}$$

The model was implemented in the following steps:

(1) The model parameters shown in Table S1 were defined in MATLAB.
(2) One of the 10 × 10 μm cells was seeded with initial biomass concentration at 50% of the critical density (i.e., 50% of X_C). The biomass aggregate progressively spreads from the center (the initial seeding position).
(3) The geometries, physics equations, and initial conditions for the hydraulic modeling and substrate mass balance were defined in MATLAB and imported into COMSOL. The initial velocity in the bulk liquid and the boundary layer was assumed to be zero. The initial substrate concentration in all the domains was the same as the bulk substrate concentration.
(4) The hydraulic model and substrate mass balance were solved in COMSOL for the time interval of 6 h (ΔT).
(5) The results from the COMSOL calculation in step 4 were exported to MATLAB and used to determine the biomass density. If the resulting biomass specific density in certain cells was larger than one, the cells were divided into two and spread according to the CA algorithm.
(6) The new biomass aggregate geometries were defined based on the result from step 5. The newly created biomass geometries were rotated 15°anti-clockwise relative to the previous biomass geometries.
(7) Steps 4 to 6 were repeated until biomass aggregate diameter of 0.7 mm was reached. For the repeated simulations, the previous result at the end of 6 h simulation was used as the initial condition for the next simulation.

The maximum mesh size for the bulk liquid and biomass aggregate was selected as 25 and 2.5 μm, respectively (Fig. S6).

To examine the effect of rotation angle on the simulation results, a sensitivity analysis was performed using the following rotation angles: 10, 20, 30, 40 and 50°. Fig. S7 in the SI displays the derived granule images and circularities produced from simulations with different rotation angles. The results in Fig. S7 show that the rotation angle had no significant effect on the biomass aggregate morphology and circularity.

The biomass aggregates of different morphologies were produced by running the model at different shear and substrate concentration conditions.

2.6. Reversed Thiele modulus

The reversed Thiele (RT) modulus, defined by the ratio of the maximum substrate transport rate to the maximum substrate reaction rate, was used to represent the condition for biomass aggregate formation:

$$\mathrm{RT} = \frac{Maxium\ substrate\ \ transport\ rate}{Maxium\ substrate\ reaction\ rate} \tag{7}$$

The substrate transport rate includes transport in the HBL and CBL, and was affected by the flow velocity and both the HBL and CBL thickness. Under a high flow velocity condition, the substrate transport in the HBL is not a limiting factor. The substrate transport was limited by the diffusion in the CBL. On the other hand, under a low flow velocity condition, both the HBL and CBL substrate transport could become a limiting factor. For the 2D simulation condition, the maximum substrate transport rate in the CBL was calculated according to Eq. (8) (Fig. S3 in SI).

$$m_{CBL} = 2\pi rD\frac{C}{L_C} \tag{8}$$

where, r is the radius of biomass aggregate; L_C is the thickness of CBL, C is the substrate concentration at the CBL border; D is the diffusion coefficient.

The maximum substrate transport rate in the HBL was calculated according to eq. (9)

$$m_{HBL} = 2\pi \mathrm{rVC} + 2\pi rD\frac{C}{L_H} \tag{9}$$

where, V is liquid velocity toward biomass aggregate, L_H is the thickness of HBL.

The smaller value from eqs. (8) and (9) was used to calculate the RT value in eq. (7).

The maximum substrate reaction rate (m_{SR}) was calculated as:

$$m_{SR} = \pi r^2 \mu \frac{C}{k + C} X \tag{10}$$

The calculated RT values under different biomass aggregate radii, substrate concentrations, and flow velocities (Fig. S8 in SI) show that the RT value decreases with increasing biomass aggregate radius, increases linearly with substrate concentration, increases with shear values below 100 s^{-1} and stabilized for shear values 200 s^{-1} and higher.

2.7. Image analysis of the biomass aggregates

The image analysis toolbox within the MATLAB software was used to measure the biomass aggregate's diameter and circularity. The diameter was assumed to be the same as a bounding circle with the minimum diameter that covered all the biomass aggregate area. The circularity (I_C) was calculated using the following equation:

$$I_C = \frac{4\pi\ area}{primeter^2} \tag{11}$$

3. Simulation results

3.1. Simulation results at two typical conditions

The biomass aggregate morphology produced under two different substrate concentrations and flow conditions is shown in Fig. 2. The flow velocity and the substrate concentration distribution (Fig. 2(a) and (b), respectively) show that under the low inlet velocity (0.01 m/s and average shear rate of 20 s^{-1}) and low bulk substrate concentration (defined as 50 S_{min}), the biomass aggregate had an irregular surface and low circularity (Fig. 2 (a, b))

Under high shear (inlet velocity 0.05 m/s and an average shear rate of 250 s^{-1}) and high substrate concentration (300 S_{min}) condition, the shape of the biomass aggregate was more circular and compact than the low shear and low substrate condition (Fig. 2 (c, d)). The high flow velocity reduced the CBL thickness shown in the Fig. 2(c), in comparison to the CBL shown in the Fig. 2(a). The reduced CBL thickness and increased substrate concentration increased the substrate flux into the biomass aggregate.

3.2. Impact of shear and substrate concentration on the biomass aggregate morphology

Fig. 3(a) displays the morphology and circularity for biomass aggregate formed under the constant bulk substrate concentration of *200* S_{min} and variable shear rate at 0-300 S^{-1}. At the zero shear condition, the biomass aggregate had an open, finger-like morphology that became more compact and circular with increasing shear rate. The impact of bulk substrate concentration

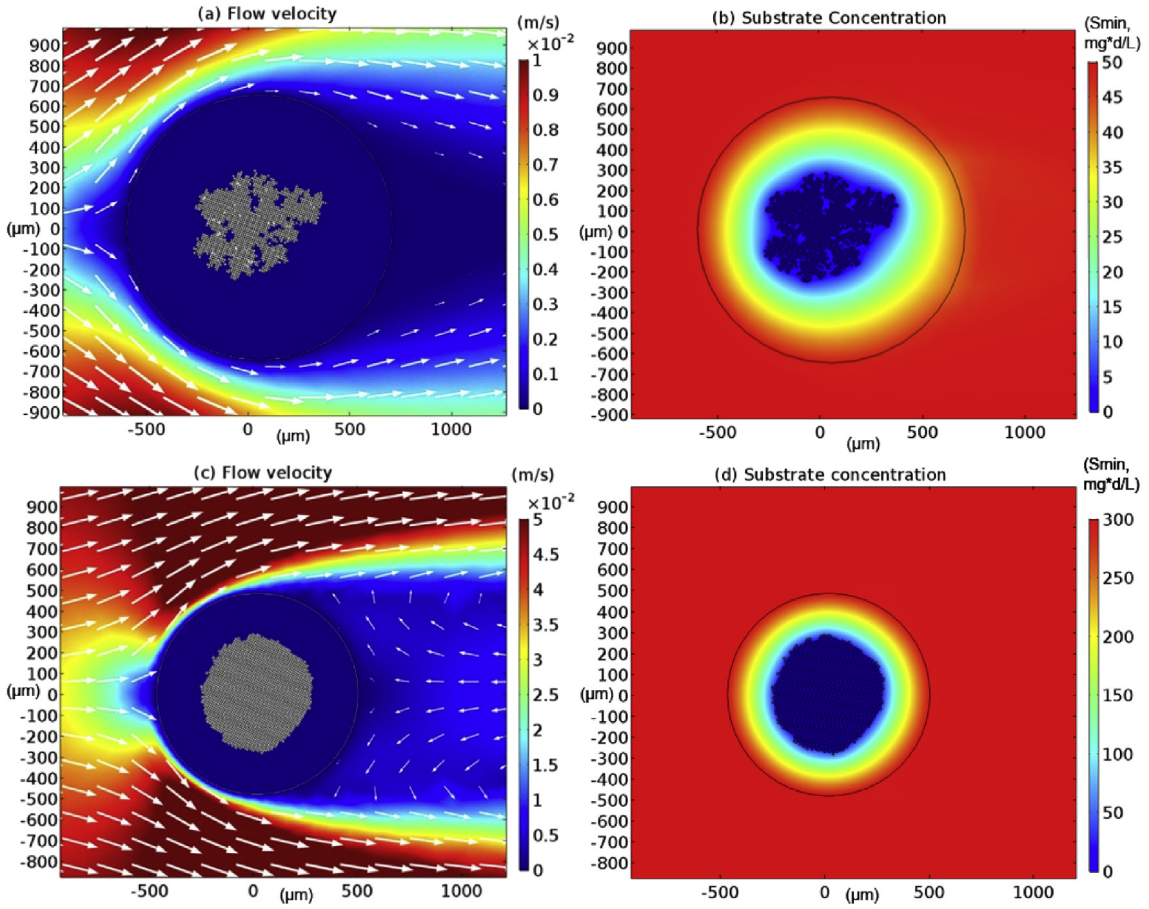

Fig. 2. (a) Biomass aggregate morphology and velocity field formed under bulk substrate concentration of 50 S_{min} and average shear rate of 20 s^{-1} condition; (b) substrate concentration distribution under bulk substrate concentration of 50 S_{min} and average shear rate of 20 s^{-1} condition; (c) biomass aggregate morphology and velocity field formed under bulk substrate concentration of 300 S_{min} and average shear rate of 250 s^{-1} condition; (d) substrate concentration distribution under bulk substrate concentration of 300 S_{min} and average shear rate of 250 s^{-1} condition.

on the biomass aggregate morphology under the constant shear rate of 200 S^{-1} is shown in Fig. 3(b). The increase in the substrate concentration from 50 to 600 S_{min} led to more compact and circular biomass aggregates. Results in Fig. 3 suggest that at some limiting value (either shear rate or bulk substrate concentration) no significant change in the circularity was observed.

To investigate the combined impact of shear and substrate concentration on the biomass aggregate morphology, a series of simulations were performed under shear rates between 0 and 250 S^{-1} and substrate concentrations between 50 and 600 S_{min}. The surface plot of the circularity from the simulations (Fig. 3(c)) shows that under low substrate concentration, i.e., less than 150 S_{min}, the circularity of biomass aggregates remained below 0.1 despite the variation of shear rate between 0 and 250 S^{-1}. For substrate concentration higher than 500 S_{min}, the biomass aggregates circularity remained larger than 0.5. In other words, the local shear has no impact on the biomass aggregate morphology for substrate concentrations less than 150 S_{min} or higher than 500 S_{min}. For substrate concentrations between 150 and 500 S_{min}, increasing shear led to high biomass aggregate circularity. High circularity is defined as values greater than 0.6, while low circularity is defined as values below 0.2.

3.3. The effect of reversed Thiele modulus on the biomass aggregate morphology

Fig. 4(a) displays the calculated RT values for different combinations of shear and bulk substrate concentration of a circular biomass aggregate with a diameter of 500 μm. In Fig. 4(a), the shape of the circularity curve as a function of the RT value was similar to the shear and substrate concentration effect shown in Fig. 3(c). This result suggests that the RT value could be used as a universal dimensionless factor to determine the morphology of biomass aggregates at different shear rates and substrate concentrations. The impact of RT values on biomass aggregates of 400, 500 and 600 μm diameter (Fig. 4(b)) show similar patterns regardless of the aggregate size. The biomass aggregate circularity increased from 0.1 to 0.65 when the RT value increased from 0.02 to 0.1, and stabilized for RT value larger than 0.1. The simulation results indicate that the maximum substrate transport rate should be around 10% of the maximum substrate reaction rate to produce biomass aggregates of circularity near 0.65.

The RT values shown in Fig. 4(b) were calculated from various arbitrary combinations of shear and bulk substrate concentration. This set of simulated experiments indicate that shear and bulk substrate concentration work in a unified way by controlling the substrate availability to affect the biomass aggregate morphology. For granule formation to be achieved, an RT value larger than 0.1 is necessary.

To understand how the biomass aggregate size affects its circularity, the development of biomass aggregate size, circularity, and the RT value for the two simulation scenarios in Fig. 2 were performed and results are shown in Fig. 5. Under the low substrate availability scenario, the increase in the floc diameter coincided

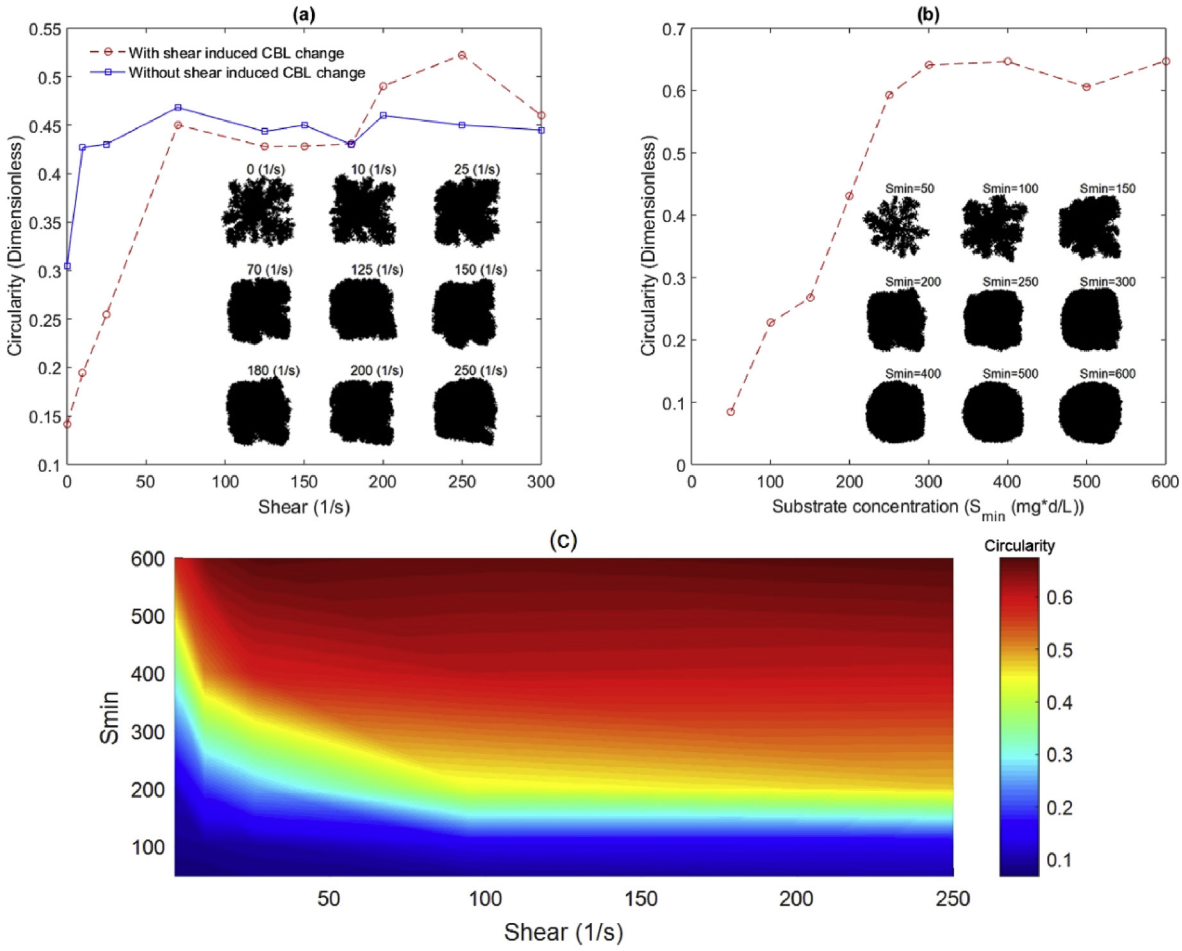

Fig. 3. (a) Morphology and circularity of biomass aggregate formed under the constant bulk substrate concentration of *200* S_{min} and variable shear rate at 0-300 S^{-1}; (b) Morphology and circularity of biomass aggregate formed under the variable bulk substrate concentration of 50-600 S_{min} and constant shear rate at 200 S^{-1}; (c) Combined impact of shear and substrate concentration on the biomass circularity.

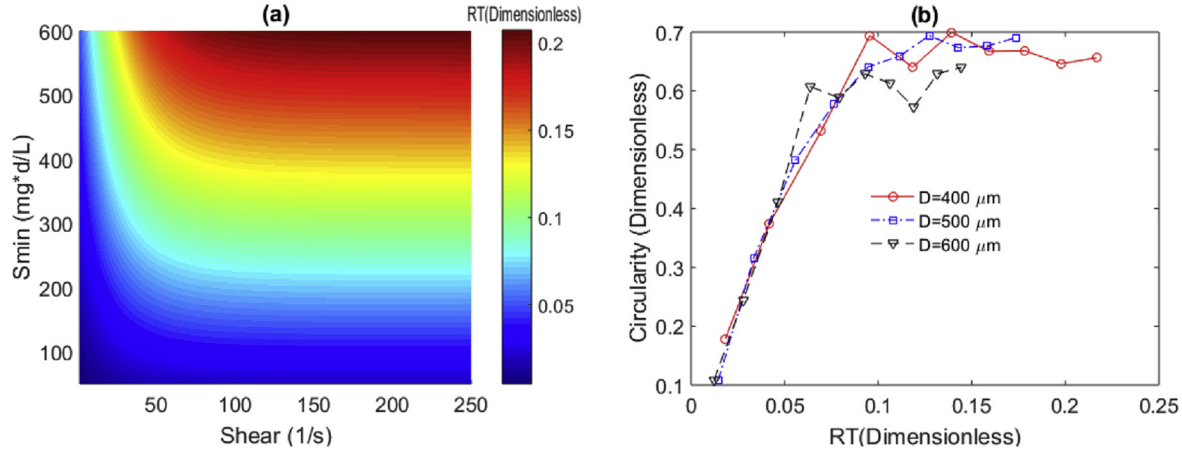

Fig. 4. (a) Calculated RT value for different combinations of substrate concentration and shear condition for a circular granule of 0.5 mm diameter; (b) The effect of RT on the circularity of biomass aggregate of 0.4, 0.5 and 0.6 mm diameter, respectively.

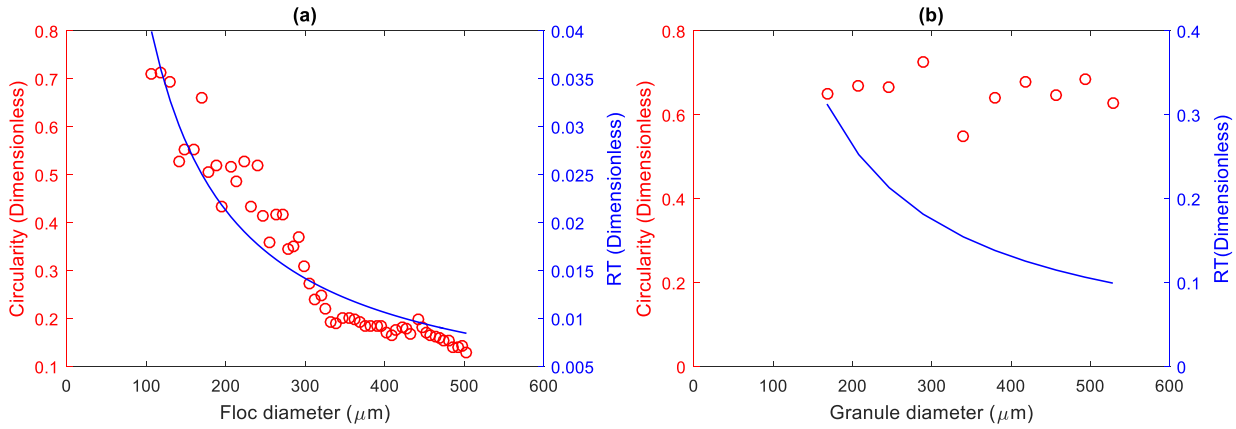

Fig. 5. (a) Development of floc diameter, circularity, and RT value for the simulation shown in Fig. 2(a, b); (b) Development of floc diameter, circularity, and RT value for the simulation shown in Fig. 2(c, d).

with a decrease in circularity and RT values (Fig. 5(a)). Under the high substrate availability scenario, the circularity was stable despite the increase in granule diameter and decrease in RT value (Fig. 5(b)). However, the RT value in Fig. 5(b) remained above 0.1 and supports the results in Fig. 4 that a high circularity could be achieved at or above this RT threshold value regardless of the biomass aggregate size. This result suggests that the RT value and not the biomass aggregate size determines its circularity.

3.4. Simulation of biomass aggregate formation and disintegration in a batch reactor

The simulation results described above were derived under constant bulk substrate concentrations and stable shear conditions. To simulate the biomass aggregate formation in a typical sequencing batch reactor (SBR), the shear and bulk substrate concentration were varied according to the profiles in Fig. 6 (a) and (b), respectively. The average shear rate variation shown in Fig. 6 (a) was achieved by adjusting the inlet velocity between 0 and 0.05 m/s using a sinusoidal function. The bulk substrate concentration decreased during each cycle according to a first-order reaction rate:

$$C(t) = C_0 e^{-kt} \quad (12)$$

For the case shown in Fig. 6 (b), the first order reaction coefficient k was set to 1 h^{-1}. Results in Fig. 6 (c) from this varying shear rate and declining bulk substrate concentration led to a declining RT value starting from a value greater than 0.1 to zero at the end of each cycle. Fig. 6 (d) displays the biomass aggregate formed under this alternating shear and declining substrate condition. The substrate concentration profile within the biomass aggregate at the end of one reaction cycle is displayed in Fig. 6 (e). The circularity for the biomass aggregate was calculated to be 0.6 when its diameter was 500 μm. Another simulation was performed that produced an alternating shear rate and a declining RT value where at no point was the RT above 0.1 (See Supplemental Fig. S9). In that simulation, the results clearly show that a floc biomass aggregate with a 0.08 circularity value was produced. It can be concluded that the biomass aggregate formed under variable shear and substrate conditions can only produce circular and compact biomass aggregate, if at some point the RT is equal or larger than 0.1 indicating sufficient substrate availability.

Fig. 5(b) suggests that for the formation of granules with circularity more than 0.6, the RT value should be greater than 0.1. The granule produced in the SBR reactor had a circularity of 0.6 and the RT value in the SBR cycle varied between 0 and 0.1. In a separate simulation, we performed a numerical test with a fast declining substrate concentration (i.e., $k = 5\ h^{-1}$ in equation (12)) (Fig. S9 **in the SI**). The RT value was initially higher than 0.1, but remained less than 0.01 for the majority of the 4 h reaction cycle (Fig. S10(c)). During this simulation, granules with circularity at 0.6 can still be produced. We hypothesize that the initial RT value above 0.1 at the start of each cycle is responsible for the granule formation in the SBR. If the SBR system never achieves this threshold value as shown in Fig. S9, granules will not be produced. One possible explanation for this requirement in SBRs is that biomass growth may be occurring during the high RT stage due to the high substrate transfer rate.

4. Discussion

4.1. The micro-environment for biomass granulation: substrate availability theory

The simulation study examined the effect of micro-environment, characterized by shear and substrate concentration in close proximity to the biomass aggregate, on the aerobic granulation process. Our results indicated that shear and substrate concentration that can be characterized by the RT value, work together to influence the occurrence of aerobic granular sludge. RT represents the ratio between the maximum substrate transport and maximum substrate reaction rate. For AGS to be formed, the RT value should be higher than 0.1. This value could be achieved by increasing the shear or substrate concentration, or both (Fig. 4 (a)).

Although the effects of shear on the biomass aggregate have been widely reported, the underlying reasons for these effects on the biomass aggregate morphology have not been clearly determined. Considering the many aspects that shear could exert on the biomass aggregates (e.g., biomass density, extracellular polymeric substances (EPS) production, substrate transport, biomass detachment (Liu and Tay, 2002)), it is very difficult to rely on a single mechanism to explain the effect of shear on the biomass aggregate morphology. In this study, we focused on the effect of shear-induced substrate transport on the biomass granulation process: (a) the shear-induced CBL thickness change and (b) the substrate transport in the HBL. The simulation results identified that shear only affected the biomass granulation process for the medium (150−500 S_{min}) range of substrate concentration. At high substrate concentrations, high shear is not necessary to increase the RT value, while an increase in shear cannot result in an increase in the RT

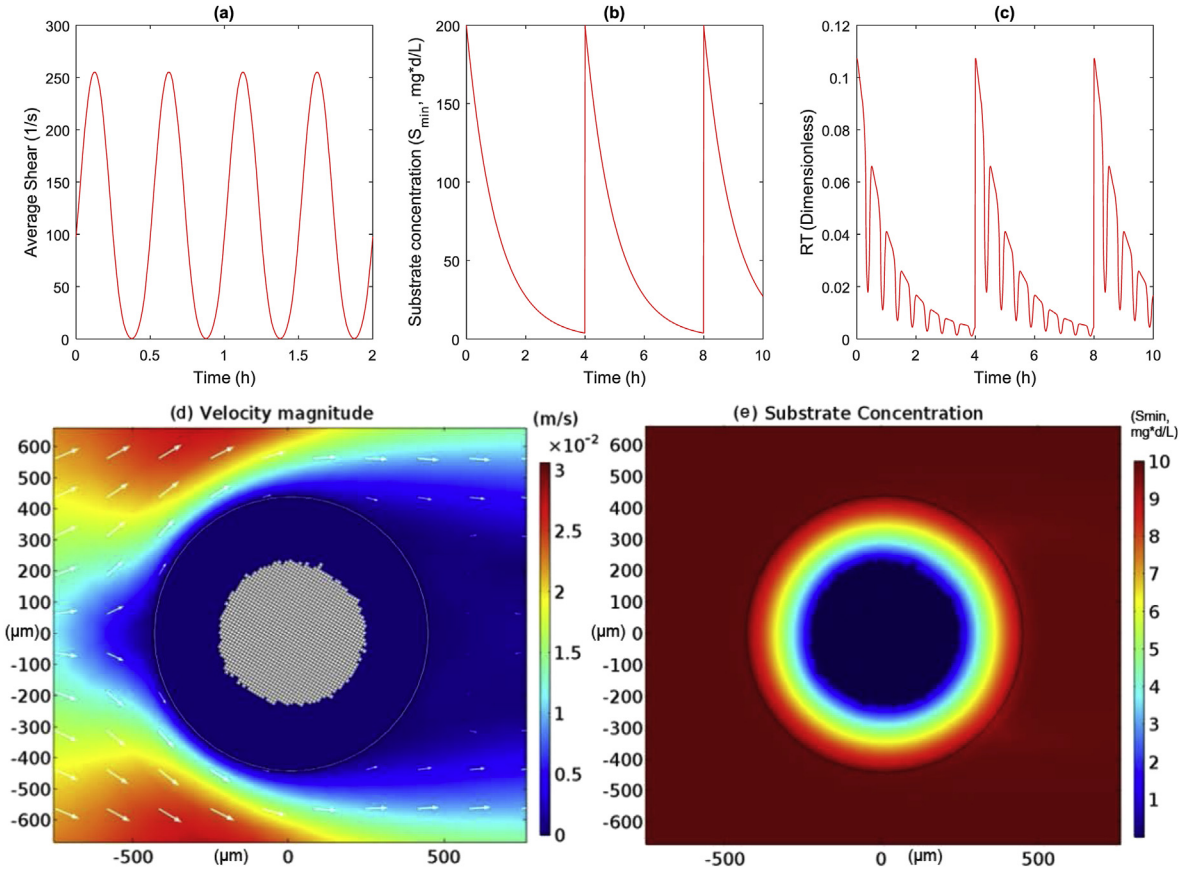

Fig. 6. (a) Variation of average shear rates, (b) Bulk substrate concentration decreasing under first order reaction rate, (c) Calculated RT value in the batch reaction cycle, (d) biomass aggregates, shear rate, and velocity field, (e) substrate concentration profile at the end of one reaction cycle.

value at very low substrate concentrations, under which the granules could not be formed. This simulation result is supported by experimental data (Sturm and Irvine, 2008), in which aerobic granules cannot be formed under low substrate concentration, despite the elevated shear force. The RT value represents how the shear and bulk substrate concentration are linked to affect the substrate availability in the micro-scale environment.

4.2. The impact of reactor macro-environment on the biomass aggregate micro-environment

Many of the prior experimental studies on granule formation were performed by adjusting reactor operational factors that influence the macro-scale level. Here, we examined how these operational factors affected the micro-environment and subsequently affected biomass aggregate morphology.

4.2.1. SBR vs Continuous flow reactor

Granules are usually more challenging to grow in a continuous flow reactor (Kent et al., 2018). The bulk substrate concentration (S_{bulk}) in the ideal continuously stirred tank reactor (CSTR) could be expressed by the following equation (Metcalf and Eddy, 2002):

$$S_{bulk} = \frac{K_S(1 + b \cdot SRT)}{SRT \cdot (\mu_{max,H} - b) - 1} \tag{13}$$

where, b is the biomass decay rate (d^{-1}). If we ignore the biomass decay rate, the above equation could be simplified to:

$$S_{bulk} = \frac{K_S}{SRT \cdot \mu_{max,H} - 1} \tag{14}$$

Considering the definition of S_{min} in the Eq. (6), the above equation could be rewritten as:

$$S_{bulk} = \frac{1}{SRT - 1/\mu_{max,H}} S_{min} \tag{15}$$

For a typical SRT of 10 d and $\mu_{max,H}$ *of 3* d^{-1} in the aerobic activated sludge system, the S_{bulk} in the CSTR could be calculated as 0.103 S_{min}. According to the simulation results (Fig. 3(c)), at such a low substrate concentration, no granule will be formed. This simple analysis could explain why aerobic granules have been rarely reported in continuous reactors (Franca et al., 2017; Kent et al., 2018; Liu and Tay, 2002). Simulation results here confirmed that granules are more easily formed in SBRs than in continuous flow reactors (Beun et al., 1999; Franca et al., 2018) due to the high initial substrate availability in the feast period of SBR operation.

4.2.2. Selection of slower growing organisms to promote granulation

It should be noted that the substrate concentration used in this study was normalized in terms of the biomass kinetic parameters, i.e., half saturation constant and maximum specific growth rate (Equation (6)). The lower maximum specific growth rate of slow-growing organisms could be equivalent to high substrate availability according to Equation (6). The simulation results also explain why slow growers are preferred in granule formation. It can be

concluded from the previous studies that slow-growing organisms are favored in the formation of granules (de Kreuk and van Loosdrecht, 2004). Long before aerobic granules were discovered, anaerobic granules have been used extensively in UASB (up-flow anaerobic sludge blanket) reactors (Lettinga, 1995). Other slow growers, e.g., the nitrifying bacteria (Kishida et al., 2012) and ANNAMOX bacteria (van der Star et al., 2008) also have a tendency to form granules. The high bulk substrate availability condition could be readily maintained for slow-growing microorganisms.

4.2.3. F/M ratio adjustment

The effect of F/M (food to microorganisms) ratio on the aerobic granulation process is inconsistent in the literature. Initial high F/M ratio (1.1 g COD g VSS^{-1} d^{-1}) was reported to promote granulation and increase the granule size. However, F/M ratio needs to be reduced (to 0.3 g COD g VSS^{-1} d^{-1}) to achieve long term granule stability (Li et al., 2011). On the other hand, decreasing F/M ratio from 0.6 to 0.1 g COD g VSS^{-1} d^{-1} was shown to increase filamentous growth and unstable granules (Liu and Liu, 2006). Others have reported that very high F/M ratio (above 2.5 g COD g VSS^{-1} d^{-1}) led to filamentous bulking and poor settling in AGS (Hamza et al., 2018).

The ability to produce granular sludge at high F/M ratio (Li et al., 2011) and the increase in filamentous growth under low F/M ratio (Hamza et al., 2018) could be explained by the low substrate availability condition shown in our simulations.

4.2.4. Aeration rate

High DO concentrations are typically required to produce round and clearly shaped aerobic granules. Low DO concentrations lead to the filamentous growth and granule instability (Sturm and Irvine, 2008), consistent with the substrate availability theory described in this study. It is usually believed that aeration could affect the aerobic granulation process by applying sufficient hydraulic shear and DO (Liu and Tay, 2002). Here we showed that shear and substrate concentration work on the same principle of increasing substrate availability for granule formation. Only organic substrate was included in the model equation to represent the limiting substrate. When the organic substrate was not the limiting substrate, high DO was required to achieve aerobic granulation (Sturm and Irvine, 2008).

4.2.5. Feast and famine condition

The feast and famine condition usually applied in the SBR was regarded as one of the main driving forces for granulation; granule formation was promoted by an extended famine period (Beun et al., 2000; Corsino et al., 2017; Franca et al., 2018).

For any given initial substrate concentration, an increase in the starvation period increased the rate of substrate availability in the feast period, therefore promoting the granulation process according to the simulation result in this study. Conversely, in the SBR where the feeding period was spread over a longer time span to reduce the bulk substrate concentration in the feast period, the biomass aggregate settling ability decreased and filamentous bacterial growth increased (Martins et al., 2003). Granules with high settling ability could not be formed under low substrate availability regardless of a feast/famine condition. This result suggests that it was the high substrate availability in the feast period that promoted granulation, not the feast/famine condition.

4.3. Implications of the simulation study on the cultivation of aerobic granules

This simulation study suggests that the microscale substrate availability characterized by the local shear and bulk substrate concentration could provide a reasonable explanation for biomass granulation formation under the model assumptions (e.g., soluble substrate conditions). The substrate availability theory could explain the majority of the operational strategies used for promoting biomass granulation, i.e., use of batch reactors, selection for slow-growing microorganisms, F/M ratio adjustment, feast and famine condition, and short settling time. The high substrate availability condition appears to be the common denominator in these strategies for biomass granulation, although more experimental verification is needed.

The substrate availability phenomenon identified in this study could lead to completely new strategies for biomass granulation, e.g., a “granule selector” with high substrate availability placed upstream of the main reactor, or additional organic substrate addition with monitoring to avoid substrate deficiency.

The study used simulation to examine the impact of shear and substrate availability on granule formation. However, biomass granulation is quite complex and could involve other factors, e.g., the interactive effects of EPS (extracellular polymer substances) in the granule formation process. Research to date has not informed investigators or practitioners on the impact of shear and substrate availability on the production of EPS or the role EPS has on floc morphology during the granulation process. Only one active biomass component was included in the model developed in this study. The actual biomass aggregates found in aerobic biological processes include multiple biomass species, i.e., heterotrophic bacteria, autotrophic bacteria, and their decay products. The mathematical model could be expanded to include the above mentioned factors, and validated by detailed experimental data to fully understand the biomass granulation process.

5. Conclusions

- Results of this in-silico study using a 2-D biofilm model based on the cellular automata algorithm and computational fluid dynamics revealed that shear and bulk substrate concentration combined to create the optimal conditions for aerobic granule formation.
- This process can be characterized by the reversed Thiele (RT) modulus value, which is the ratio of the maximum substrate transport over the maximum substrate reaction rate and an indicator of substrate availability. For AGS formation, the RT value should be greater than 0.1.
- The RT value proposed in this study could also explain why granules could be more readily formed in an SBR (with a high initial RT value) than in a CSTR (with a low RT value). Many common strategies for biomass granulation production, such as the use of batch reactors, selection for slow-growing microorganism, F/M ratio adjustment, feast and famine condition, and short settling time, etc., can be explained using the RT value and further suggests possible new strategies for AGS formation.

Declaration of competing interest

The authors declare that they have no known competing financial interests or personal relationships that could have appeared to influence the work reported in this paper.

Acknowledgement

The study is supported by the Natural Science Foundation of China (Grant No. 51478410) and US National Science Foundation (CBET Grant No. 1805666).

Appendix A. Supplementary data

Supplementary data to this article can be found online at https://doi.org/10.1016/j.watres.2019.115384.

References

Beun, J.J., Hendriks, A., van Loosdrecht, M.C.M., Morgenroth, E., Wilderer, P.A., Heijnen, J.J., 1999. Aerobic granulation in a sequencing batch reactor. Water Res. 33 (10), 2283–2290.

Beun, J.J., van Loosdrecht, M.C., Heijnen, J.J., 2002. Aerobic granulation in a sequencing batch airlift reactor. Water Res. 36 (3), 702–712.

Beun, J.J., Van Loosdrecht, M.C.M., Heijnen, J.J., 2000. Aerobic Granulation, pp. 41–48.

Bishop, P.L., Gibbs, J.T., Cunningham, B.E., 1997. Relationship between concentration and hydrodynamic boundary layers over biofilms. Environ. Technol. 18 (4), 375–385.

Corsino, S.F., di Biase, A., Devlin, T.R., Munz, G., Torregrossa, M., Oleszkiewicz, J.A., 2017. Effect of extended famine conditions on aerobic granular sludge stability in the treatment of brewery wastewater. Bioresour. Technol. 226, 150–157.

de Kreuk, M.K., Heijnen, J.J., van Loosdrecht, M.C., 2005. Simultaneous COD, nitrogen, and phosphate removal by aerobic granular sludge. Biotechnol. Bioeng. 90 (6), 761–769.

de Kreuk, M.K., van Loosdrecht, M.C., 2004. Selection of slow growing organisms as a means for improving aerobic granular sludge stability. Water Sci. Technol. 49 (11–12), 9–17.

Franca, R.D.G., Pinheiro, H.M., van Loosdrecht, M.C.M., Lourenço, N.D., 2017. Stability of aerobic granules during long-term bioreactor operation. Biotechnol. Adv.

Franca, R.D.G., Pinheiro, H.M., van Loosdrecht, M.C.M., Lourenço, N.D., 2018. Stability of aerobic granules during long-term bioreactor operation. Biotechnol. Adv. 36 (1), 228–246.

Hamza, R.A., Sheng, Z., Iorhemen, O.T., Zaghloul, M.S., Tay, J.H., 2018. Impact of food-to-microorganisms ratio on the stability of aerobic granular sludge treating high-strength organic wastewater. Water Res. 147, 287–298.

Kent, T.R., Bott, C.B., Wang, Z.-W., 2018. State of the art of aerobic granulation in continuous flow bioreactors. Biotechnol. Adv. 36 (4), 1139–1166.

Kishida, N., Saeki, G., Tsuneda, S., Sudo, R., 2012. Rapid start-up of a nitrifying reactor using aerobic granular sludge as seed sludge. Water Sci. Technol. 65 (3), 581–588.

Lettinga, G., 1995. Anaerobic digestion and wastewater treatment systems. Antonie Leeuwenhoek 67 (1), 3–28.

Li, A.-j., Li, X.-y., Yu, H.-q., 2011. Effect of the food-to-microorganism (F/M) ratio on the formation and size of aerobic sludge granules. Process Biochem. 46 (12), 2269–2276.

Li, B., Bishop, P.L., 2004. Micro-profiles of activated sludge floc determined using microelectrodes. Water Res. 38 (5), 1248–1258.

Liu, Y., Liu, Q.-S., 2006. Causes and control of filamentous growth in aerobic granular sludge sequencing batch reactors. Biotechnol. Adv. 24 (1), 115–127.

Liu, Y., Tay, J.-H., 2002. The essential role of hydrodynamic shear force in the formation of biofilm and granular sludge. Water Res. 36 (7), 1653–1665.

Liu, Y., Xu, H.-L., Yang, S.-F., Tay, J.-H., 2003. Mechanisms and models for anaerobic granulation in upflow anaerobic sludge blanket reactor. Water Res. 37 (3), 661–673.

Martins, A.M.P., Heijnen, J.J., van Loosdrecht, M.C.M., 2003. Effect of feeding pattern and storage on the sludge settleability under aerobic conditions. Water Res. 37 (11), 2555–2570.

Metcalf, Eddy, 2002. Wastewater Engineering : Treatment and Reuse. McGraw-Hill.

Nancharaiah, Y.V., Reddy, G.K.K., 2018. Aerobic granular sludge technology: mechanisms of granulation and biotechnological applications. Bioresour. Technol. 247, 1128–1143.

Picioreanu, C., van Loosdrecht, M.C.M., Heijnen, J.J., 1998. Mathematical modeling of biofilm structure with a hybrid differential-discrete cellular automaton approach. Biotechnol. Bioeng. 58 (1), 101–116.

Pronk, M., de Kreuk, M.K., de Bruin, B., Kamminga, P., Kleerebezem, R., van Loosdrecht, M.C.M., 2015. Full scale performance of the aerobic granular sludge process for sewage treatment. Water Res. 84, 207–217.

Stoodley, P., deBeer, D., Lewandowski, Z., 1994. Liquid flow in biofilm systems. Appl. Environ. Microbiol. 60 (8), 2711–2716.

Stoodley, P., Lewandowski, Z., Boyle, J.D., Lappin-Scott, H.M., 1999. Structural deformation of bacterial biofilms caused by short-term fluctuations in fluid shear: an in situ investigation of biofilm rheology. Biotechnol. Bioeng. 65 (1), 83–92.

Sturm, B.S., Irvine, R.L., 2008. Dissolved oxygen as a key parameter to aerobic granule formation. Water Sci. Technol. 58 (4), 781–787.

van der Star, W.R.L., Miclea, A.I., van Dongen, U.G.J.M., Muyzer, G., Picioreanu, C., van Loosdrecht, M.C.M., 2008. The membrane bioreactor: a novel tool to grow anammox bacteria as free cells. Biotechnol. Bioeng. 101 (2), 286–294.

Wanner, O., Morgenroth, E., 2004. Biofilm modeling with AQUASIM. Water Sci. Technol. 49 (11–12), 137–144.